NANO LETTERS

2008
Vol. 8, No. 10
3456-3460

Single and Tandem Axial *p-i-n* Nanowire Photovoltaic Devices

Thomas J. Kempa,[†,⊥] Bozhi Tian,[†,⊥] Dong Rip Kim,[‡] Jinsong Hu,[†] Xiaolin Zheng,[*,‡] and Charles M. Lieber[*,†,§]

Department of Chemistry and Chemical Biology, Harvard University, Cambridge, Massachusetts 02138, Department of Mechanical Engineering, Stanford University, Stanford, California 94305, School of Engineering and Applied Science, Harvard University, Cambridge, Massachusetts 02138

Received August 1, 2008; Revised Manuscript Received August 24, 2008

ABSTRACT

Nanowires represent a promising class of materials for exploring new concepts in solar energy conversion. Here we report the first experimental realization of axial modulation-doped p-i-n and tandem p-i-n$^+$−p$^+$-i-n silicon nanowire (SiNW) photovoltaic elements. Scanning electron microscopy images of selectively etched nanowires demonstrate excellent synthetic control over doping and lengths of distinct regions in the diode structures. Current−voltage ($I-V$) characteristics reveal clear and reproducible diode characteristics for the p-i-n and p-n SiNW devices. Under simulated one-sun solar conditions (AM 1.5G), optimized p-i-n SiNW devices exhibited an open circuit voltage (V_{oc}) of 0.29 V, a maximum short-circuit current density of 3.5 mA/cm^2, and a maximum efficiency of 0.5%. The response of the short-circuit current versus V_{oc} under varying illumination intensities shows that the diode quality factor is improved from $n = 1.78$ to $n = 1.28$ by insertion of the i-type SiNW segment. The temperature dependence of V_{oc} scales as −2.97 mV/K and extrapolates to the crystalline Si band gap at 0 K, which is in excellent agreement with bulk properties. Finally, a novel single SiNW tandem solar cell consisting of synthetic integration of two photovoltaic elements with an overall p-i-n$^+$−p$^+$-i-n structure was prepared and shown to exhibit a V_{oc} that is on average 57% larger than that of the single p-i-n device. Fundamental studies of such well-defined nanowire photovoltaics will enable their intrinsic performance limits to be defined.

There is currently considerable effort exploring inorganic nanostructures as key components of or as stand-alone photovoltaic devices.[1−6] For example, the ability to control through synthesis the structure and composition of semiconductor nanowires and nanocrystals make them attractive building blocks for understanding factors determining and potentially improving photovoltaic device efficiency.[1,2,4,5] In this context, our group[4] and others[5,6] have explored photovoltaic elements configured from chemically synthesized SiNWs. We have reported investigations of single coaxial p-type/intrinsic/n-type SiNWs[4] in which the intervening intrinsic shell was tuned to yield short circuit current densities (J_{sc}) and efficiencies up to 23.9 mA/cm^2 and to 3.4%, respectively, under 1-sun AM 1.5G illumination.[4] In a related approach, p-SiNWs were coated with an n-type amorphous silicon shell to yield diodes with $J_{sc} \sim 1.7$ mA/cm^2 and an efficiency of ∼0.1% for AM 1.5G illumination.[5] Rectifying metal contacts to unintentionally doped SiNWs have also been exploited to define single nanowire photovoltaic devices with J_{sc} and efficiency values of ∼5.0 mA/cm^2 and 0.5%, respectively, for AM 1.5G illumination.[6] These studies highlight unique opportunities for integrated nanowire photovoltaic elements, yet as might be expected, the initial results show lower performance than state-of-the-art planar silicon devices.

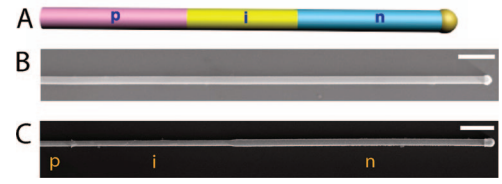

Figure 1. Scheme and structural characterization of axial p-i-n Si NWs. (A) Schematic of an axially modulated p-i-n SiNW. Growth is mediated with Au catalyst (gold-colored hemisphere) in a sequence beginning with p-, i-, and ending with n-regions. (B) SEM image of a uniform p-i-n axial SiNW with Au catalyst ($d = 250$ nm) visible on the right-end. (C) SEM images of a p-i-n axial NW after selective wet etching. The p- and i-type Si regions have faster etching rates than the n-type region (see text for more details). Scale bars are 1 μm.

To explore further and understand factors that might be limiting nanowire photovoltaic devices reported to date, we have undertaken and report herein investigations of the properties of single p-type/intrinsic/n-type axially modulated SiNW structures (Figure 1A). In these nanostructures, key

* To whom correspondence should be addressed. E-mail: (X.L.Z.) xlzheng@stanford.edu; (C.M.L.) cml@cmliris.harvard.edu.
† Department of Chemistry and Chemical Biology, Harvard University.
‡ Department of Mechanical Engineering, Stanford University.
§ School of Engineering and Applied Science, Harvard University.
⊥ These authors contributed equally to this work.

10.1021/nl8023438 CCC: $40.75
Published on Web 09/03/2008

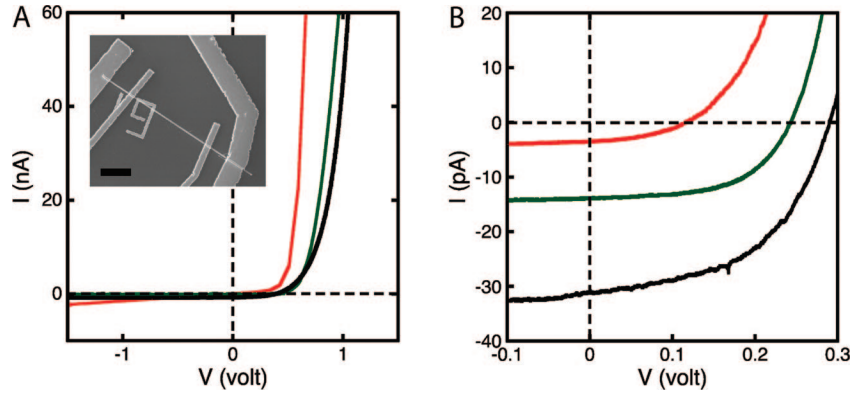

Figure 2. Transport properties of p-n and p-i-n diodes. (A) Dark $I-V$ characteristics of p-i-n SiNWs with different *i*-region lengths; red, green, and black curves correspond to i-segment lengths of 0, 2, and 4 μm, respectively. (Inset) SEM image of p-i-n SiNW device with i-length of 2 μm; scale bar is 4 μm. (B) Light $I-V$ characteristics for the i-length = 0, 2, and 4 μm devices in panel A; the illumination intensity was 100 mW/cm^2, AM 1.5G.

factors that determine device properties, including the dopant concentrations in the p- and n-type regions and the length of the intrinsic region, are all readily controlled during NW synthesis. This minimizes the need for top-down processing, which in this work is used only to define metal contacts to the terminal p- and n-type regions of the SiNWs. Hence, it is possible to assess directly the interplay of materials synthesis and device properties independent of conventional high-temperature processing such as dopant diffusion.[7]

Axial p-type/intrinsic/n-type single crystal SiNWs were synthesized via the Au-nanoparticle catalyzed vapor−liquid−solid (VLS) growth method, where axial modulation was achieved by switching dopant precursor gases at different times during elongation of the NW.[8−10] Field-emisssion scanning electron microscopy (SEM) imaging shows that the as-grown p-i-n SiNWs are straight, have smooth surfaces, and a uniform diameter with <1% deviation along the typical 25 μm length (Figure 1B). The lengths of the SiNWs are consistent with expectations based on the independently calibrated growth rates for p-, i-, and n-type SiNWs prepared under similar conditions, and thus the overall length can serve as a quick measure of the successful synthesis of the designed p-i-n structures. In addition, the uniform diameters demonstrate that axial growth is the predominant process for our experimental conditions, although careful transmission electron microscopy (TEM) analysis also shows the presence of a thin 1−3 nm amorphous shell on the single crystal silicon core that may reflect a component of radial growth. Since a thin shell could lead to current leakage in axial p-i-n diodes, the amorphous material was removed by oxidation and etching prior to device fabrication,[11] where removal was verified by TEM.

To verify successful encoding of designed p-i-n structures, the SiNWs were wet etched in potassium hydroxide solution,[12] where control studies of homogeneous single-crystal SiNWs showed that the Si etching rate, R, goes as $R_i > R_p > R_n$. SEM images of etched p-i-n SiNW structures (Figure 1C) show clear delineation of the individual regions of the diode structure, which can be referenced to the Au nanocluster catalyst at the end of the last (n-type) segment. The SiNW etching profile follows the order in which dopants were introduced during synthesis: first boron for p-type, no dopant for i-type, and then phosphorus for n-type. In addition, the length of the i-region highlighted through this procedure, 4.3 μm (Figure 1C), yields an i-region growth rate of ~1 μm/min that is consistent with studies of homogeneous *i*-SiNWs. Thus, we conclude that our approach yields single-crystal p-i-n SiNWs with controlled and reproducible encoding of different doped segments needed to produce well-defined diode structures.

The electrical transport properties of the axial p-i-n SiNW devices were first characterized by $I-V$ measurements under dark conditions at room temperature.[13] Dark $I-V$ characteristics recorded from devices with i-region lengths of 0, 2, and 4 μm are shown in Figure 2A. The lengths of the i-regions for each type of NW device were confirmed by SEM imaging of etched structures using the selective chemical etching procedure described above. Overall, these data show well-defined reverse bias current rectification, which is characteristic of the diode structure, and a current onset in forward bias at ca. 0.6 V. The onset value is typical for a p-n silicon diode with the built-in potential being established as the difference between the Fermi energies in the p- and n-type regions.[14] $I-V$ curves recorded across the p- or n-segments alone in p-i-n SiNW devices containing multiple contacts (inset, Figure 2A) showed linear behavior, thus confirming that the contacts are ohmic and that current rectification is due to the built-in electric field across the p-n junction. We also note that the reverse bias leakage current ($V < -1$ V) is largest for the p-n SiNW diodes. This leakage can be attributed to larger interfacial recombination in the p-n diodes that is reduced with inclusion of an i-region in the p-i-n SiNWs.

The photovoltaic properties of the axial p-i-n SiNW diodes were characterized under 1-sun AM 1.5G illumination. Representative light $I-V$ data for p-n, p-i-n $i = 2$ μm, and p-i-n $i = 4$ μm devices (Figure 2B) yield V_{oc} and short-circuit current, I_{sc}, values of 0.12 V and 3.5 pA, 0.24 V and 14.0 pA, and 0.29 V and 31.1 pA, respectively. The results show a systematic improvement in both V_{oc} and I_{sc} with increasing i-segment length, where the largest increase is observed in moving from the p-n to p-i-n structural motif. Qualitatively,

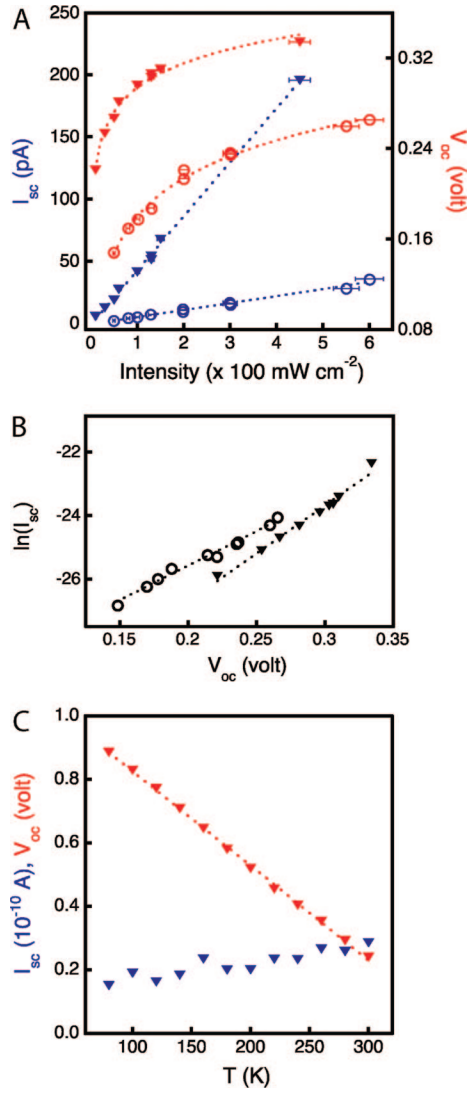

Figure 3. Photophysical characterization of p-n and p-i-n ($i = 4$ μm) axial SiNW devices. (A) V_{oc} (red) and I_{sc} (blue) for p-n (open circles) and p-i-n (filled triangles) devices as a function of AM 1.5G solar intensity (1 sun = 100 mW/cm^2). Lines through the I_{sc} and V_{oc} data correspond to guides to linear and logarithmic dependencies, respectively.[18] (B) ln(I_{sc}) vs V_{oc} for p-n (open circles) and p-i-n (filled triangles) devices where points are from data in (A). The lines correspond to fits to the ideal diode equation.[18] (C) Plots of V_{oc} (red) and I_{sc} (blue) vs temperature for a p-i-n ($i = 4$ μm) device. The line through the V_{oc} data corresponds to a linear fit.

these observations are consistent with noticeably larger leakage for the p-n devices in Figure 2A and previous studies of SiNW avalanche photodiodes[15] that identified the intrinsic region as the most optically sensitive device region. The fill-factor, FF, for the $i = 4$ μm device is 51% and yields a maximum power output per nanowire of 4.6 pW. This value is about 15 times smaller than that we achieved previously at 1-sun illumination using coaxial p-i-n SiNW devices,[4] but still ca. 1000 times larger than achieved with single piezoelectric nanowires.[16] In addition, we estimate that the AM 1.5G efficiency, η, based on the projected active area of the $i = 4$ μm device is 0.5%,[17] which is similar to the 0.46% value reported for single SiNWs with metal/semiconductor junctions,[6] but considerably smaller than the 3.4% achieved in coaxial SiNW devices.[4] The short circuit current density calculated using the same projected active area[17] is ~3.5 mA/cm^2, slightly smaller than that reported for rectifying single metal/SiNW photovoltaic devices (~5.0 mA/cm^2), although the NW diameter in the latter was 4× larger, ~1 μm.[6] We believe that the projected active area provides the best measure of the intrinsic device efficiency and J_{sc}; however, a lower bound for these values can also be obtained by considering the total projected area of the SiNW device between the p- and n- contacts.[17] For the p-i-n ($i = 4$ μm) device above, the lower limits of efficiency and J_{sc} are 0.15% and 1.4 mA/cm^2, respectively.

To characterize further the axial p-i-n SiNW photovoltaic devices, we have investigated the light intensity and temperature dependencies of the output properties. Representative I_{sc} and V_{oc} data for p-n and p-i-n devices recorded with illumination intensities from ~0.1 to 6 suns (Figure 3A) exhibit linear (I_{sc}) and logarithmic (V_{oc}) dependencies on intensity as expected for a diode structure.[18] In the case of the p-i-n SiNW photovoltaic device, we note that I_{sc} and V_{oc} increase to ~200 pA and 0.33 V, respectively, at 4.5 suns intensity and yield a maximum power of 31 pW, which is 6.7 times larger than at 1-sun. This stable increase in output power under concentrated (>1-sun) illumination is an attractive feature suggesting the promise of stand-alone nanowire photovoltaic devices[4] and is distinct from hybrid systems utilizing organic dyes or polymers with inorganic nanostructures.[19,20]

In addition, plots of ln(I_{sc}) versus V_{oc} (Figure 3B) exhibit a linear dependence with the slope proportional to the diode ideality factor (n) and intercept yielding the saturation current (I_0).[18] Analysis of these data for the p-n and p-i-n SiNW diodes yields $n = 1.78$ and 1.28, respectively, and $I_0 = 102$ and 6.14 fA, respectively. These results demonstrate that introduction of the i-region dramatically reduces the saturation current, and thus a large component of the leakage current in the diode. The lower leakage current improves the quality of the diode, which is reflected in the lower value of n, and leads to the observed larger V_{oc} due to reduced shunt losses at the junction.

Typical temperature dependent V_{oc} and I_{sc} data for a p-i-n ($i = 4$ μm) SiNW device are shown in Figure 3C. V_{oc} exhibits well-defined linear dependence on temperature with a slope of −2.97 mV/K. Extrapolation of V_{oc} to the 0 K limit yields a value of 1.12 V that is in agreement with the band gap of single crystalline silicon, $E_g = 1.123$ eV.[14] In addition, I_{sc} increases weakly with temperature (Figure 3C) due to a decrease in band gap with increasing temperature.[21] In contrast, preliminary data recorded from p-n SiNW devices exhibit more complex, nonlinear behavior suggestive of enhanced recombination at the p-n junction, assuming all other recombination processes (e.g., at the NW surface) are similar to those in the p-i-n SiNW devices. The low temperature data further confirm that insertion of the i-segment is critical to improving the junction quality. Nevertheless, there remains significant room for increasing V_{oc} in SiNW p-i-n devices at room-temperature in comparison

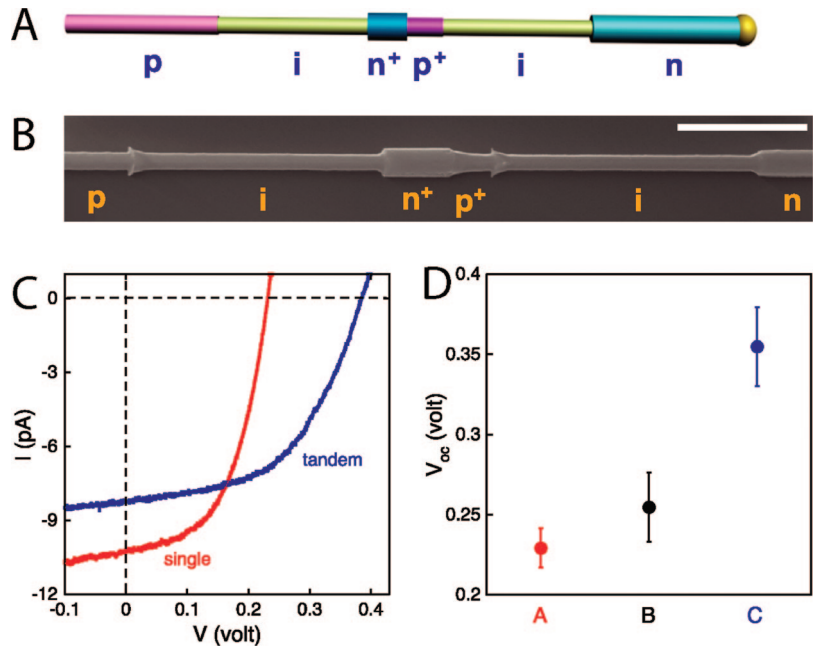

Figure 4. Tandem axial SiNW photovoltaic devices. (A) Schematic of two p-i-n diodes integrated in series on a single NW. (B) SEM images of a selectively etched tandem p-i-n^+−p^+-i-n SiNW; scale bar is 1 μm. (C) $I-V$ responses recorded on p-i (2 μm) -n (red) and p-i-n^+−p^+-i-n, $i = 2$ μm (blue) SiNW devices under AM 1.5G illumination. (D) V_{oc} for p-i (2 μm) -n (red), p-i (4 μm) -n (black), and p-i-n^+−p^+-i-n, $i = 2$ μm (blue) axial SiNW devices. Error bars are ± 1 standard deviation.

to conventional single and polycrystalline planar devices whose V_{oc} is typically 0.6−0.7 V.[7]

The optimized V_{oc} values for the p-i-n axial SiNW devices, 0.29 V, can be compared to other recent reports for single SiNW photovoltaics, including SiNW/metal junction devices,[6] 0.19 V, and coaxial p-i-n SiNW devices, 0.26 V.[4] It is interesting to note the similar V_{oc} values despite the very different SiNW diode junction geometries. This is most striking in comparison of the p-i-n axial versus coaxial SiNW devices where the junction areas differ by a factor of ~50−200 while the V_{oc}'s differ by only 10%. While the much higher saturation current ($I_0 = 3.24$ pA) for a radial p-i-n SiNW device[4] versus the present axial p-i-n SiNW device ($I_0 = 6.14$ fA) reflects greater interfacial recombination in the former, the resultant effect on V_{oc} is clearly not dominated exclusively by this factor. Rather, the similarity in V_{oc} suggests that the same physical phenomena (e.g., strong surface recombination) may be responsible for suppressing the absolute V_{oc} in both the axial and radial PV devices. Studies that identify and address the origin of the lower V_{oc}'s in both junction architectures, for example, through systematic synthetic variations in junction structure and surface passivation, are currently in progress.

Beyond addressing the question of V_{oc} in single junction devices, we have explored the potential of our approach to integrate two single-junction photovoltaic elements, in series, on a single SiNW through designed synthesis. In analogy to planar tandem-cells,[7,22,23] we synthesized SiNWs with a p-i-n^+−p^+-i-n axial modulation (Figure 4A).[10] Notably, SEM images of selectively etched SiNWs prepared in this manner (Figure 4B) demonstrate unambiguously the successful realization of the p-i-n^+−p^+-i-n axial modulation. The heavily doped n^+ and p^+ regions are readily identifiable because of their positions in the tandem device, reduced degree of etching, and expected lengths (~0.5 μm). These results confirm that our synthetic approach can yield the desired tandem junction sequence and allows precise control over the length of the doped regions.

Representative $I-V$ data recorded on p-i (2 μm) -n single and p-i-n^+−p^+-i-n, $i = 2$ μm tandem SiNW devices under AM 1.5G illumination (Figure 4C) yield characteristic V_{oc} and I_{sc} values of 0.23 V and 10.2 pA, and 0.39 V and 8.2 pA, respectively. The data demonstrate a substantial increase in V_{oc} for the tandem SiNW photovoltaic device. Moreover, analyses from measurements made on a number of devices (Figure 4D) show that the mean V_{oc} taken for a sample of $N = 10$ p-i-n^+−p^+-i-n PV devices is 0.36 ± 0.03 V, which represents a 57% increase over the value for p-i-n ($i = 2$ μm), 0.23 ± 0.01 V, and a 39% increase over p-i-n ($i = 4$ μm) 0.26 ± 0.02 V devices. The power output of the tandem device is 3.2 pW as compared to 2.3 pW for the p-i-n ($i = 2$ μm) single cell, a 39% increase. Treating the tunnel junction (heavily doped p^+/n^+) ideally, one would expect the V_{oc} to be double that of the single cell and the I_{sc} to remain constant. The smaller than ideal increase in V_{oc} and output power can be attributed to parasitic series resistances due in large part to a nonideal tunneling interface between the n^+ and p^+ segments. However, we stress the ability to integrate at high density on a single SiNW multiple p-i-n diodes to show in principle that voltage and output power can be scaled. While future studies will be needed to enhance further the V_{oc} from these SiNW tandem cells, we believe that the approach is quite promising and illustrative of the power of designed nanostructure synthesis.

In summary, we have demonstrated the first experimental realization of axial modulation-doped p-i-n and tandem p-i-

n^+-p^+-i-n SiNW photovoltaic elements. SEM imaging of selectively etched nanowires demonstrates excellent synthetic control over doping and lengths of distinct regions in the diode structures, and $I-V$ characteristics reveal clear and reproducible diode characteristics for the p-i-n and p-n SiNW devices. Under simulated, one-sun illumination, optimized p-i-n SiNW devices exhibited a V_{oc} of 0.29 V, a maximum short-circuit current density of 3.5 mA/cm^2, and maximum efficiency of 0.5%. The response of the short-circuit current versus V_{oc} under varying illumination intensities shows that the diode quality factor is improved from $n = 1.78$ to $n = 1.28$ by insertion of the i-type SiNW segment, and temperature-dependent measurements showed that V_{oc} extrapolates to bulk silicon band gap at 0 K in the p-i-n axial NW devices. Finally, a novel single SiNW tandem solar cell consisting of the designed synthesis of two series-integrated photovoltaic elements with an embedded p-i-n^+-p^+-i-n structure on a single SiNW was realized and shown to exhibit a V_{oc} that is on average 57% larger than the equivalent single junction p-i-n device. Fundamental studies of well-defined modulation-doped NW photovoltaics should enable the intrinsic limits of nanoscale elements to be defined, and such elements hold substantial promise as building blocks for the development of nanoscale solar energy conversion systems.

Acknowledgment. T.J.K acknowledges support from the NSF Graduate Research Fellowship. D.R.K. acknowledges support from the Link Foundation Energy Fellowship. X.L.Z. acknowledges the Center of Integrated Systems at Stanford University and the DARPA/YFA program for support of this work. C.M.L. acknowledges the Air Force Office of Scientific Research and a contract from MITRE Corporation for support of this work.

References

(1) Gur, I.; Fromer, N. A.; Geier, M. L.; Alivisatos, A. P. *Science* **2005**, *310*, 462.
(2) Kayes, B. M.; Atwater, H. A.; Lewis, N. S. *Appl. Phys. Lett.* **2005**, *97*, 114302.
(3) Luque, A.; Marti, A.; Nozik, A. J. *MRS Bulletin* **2007**, *32*, 236.
(4) Tian, B.; Zheng, X.; Kempa, T. J.; Fang, Y.; Yu, N.; Yu, G.; Huang, J.; Lieber, C. M. *Nature* **2007**, *449*, 885.
(5) Tsakalakos, L.; Balch, J.; Fronheiser, J.; Korevaar, B. A.; Sulima, O.; Rand, J. *Appl. Phys. Lett.* **2007**, *91*, 233117.
(6) Kelzenberg, M. D.; Turner-Evans, D. B.; Kayes, B. M.; Filler, M. A.; Putnam, M. C.; Lewis, N. S.; Atwater, H. A. *Nano Lett.* **2008**, *8*, 710.
(7) Luque, A.; Hegedus, S. *Handbook of Photovoltaic Science and Engineering*; Wiley: Chichester, 2003.
(8) Wagner, R. S.; Ellis, W. C. *Appl. Phys. Lett.* **1964**, *4*, 89.
(9) Zheng, G. F.; Lu, W.; Jin, S.; Lieber, C. M. *Adv. Mater.* **2004**, *16*, 1890.
(10) The growth substrate consisted of 250 nm Au nanoparticles immobilized on poly-L-lysine treated 600 nm SiO_2/Si slivers. The chamber temperature and pressure were held constant at 450 °C and 40 torr, respectively, and the precursor gases silane (2 sccm), dioborane (5 sccm, 100 ppm), and phosphine (1 sccm, 1000 ppm) were introduced as appropriate to form intrinsic, p-type, and n-type regions on the axial NW. The carrier gas was H_2 (60 sccm). Under these conditions and NW diameter in the range of 200−250 nm, the growth rate is ~1 μm/min. The dopant feed-in ratios (Si−B/P) were 2000:1 for both p- and n-type segments. For the tandem structures, the two i-segments were 2 μm long, the n^+ and p^+ regions were 0.5 μm in length, and the Si−B/P ratios were both 500:1 in the heavily doped n^+ and p^+ regions.
(11) SiNW devices were fabricated on silicon substrates (Nova Electronic Materials, n-type 0.005 Ω cm) with 100 nm thermal oxide and 200 nm silicon nitride at the surface. After dispersing SiNWs on the substrate, they were oxidized in a UV/O_3 dry-stripper (Samco International Inc.; Model UV-1) at 300 °C with an O_2 flow of 1 L/min. The oxide was removed by submerging the substrates in commercial buffered hydrogen fluoride (BHF) solution (Transene Company Inc.) for 5 s.
(12) SiNWs were etched with BHF for 7 s and then immersed in a 60 °C KOH/isopropanol solution (20 wt % KOH in water; 3:1 vol/vol) for 7 s. SEM studies reveal that the etching rate for i-type Si is similar to that for p-type, leading to a 52% and 46%, respectively, reduction in the original diameter for above conditions, while there is negligible etching for n-type Si.
(13) Devices were defined by electron-beam lithography followed by Ti/Pd (5 nm/250 nm) contact deposition in a thermal evaporator. $I-V$ data were recorded using an Agilent semiconductor parameter analyzer (Model 4156C) and standard solar illumination was provided by a Newport Solar Simulator (Model 96000) with air mass global, AM 1.5G filter. Illumination intensities were calibrated (100 mW/cm^2 = 1 sun) with a power meter (Coherent, Field Master). For temperature dependent experiments (Figure 3C), the probe station (Desert Cryogenics, Model TTP4) tip and substrate temperatures (LakeShore, Model 331 temperature controller) were within 5% of each other.
(14) Sze, S. M. *Physics of Semiconductor Devices*, 2nd edition; John Wiley & Sons: New York, 2004.
(15) Yang, C.; Barrelet, C. J.; Capasso, F.; Lieber, C. M. *Nano Lett.* **2006**, *6*, 2929.
(16) Wang, Z. L.; Song, J. *Science* **2006**, *312*, 242.
(17) The projected area used to calculate efficiency was approximated as the length of the intrinsic region and the depletion widths in the p- and n- regions multiplied by the NW diameter. If the entire length between the contacts of the p-i (4 μm) -n axial device was used to estimate area, the efficiency would be 0.15% and $J_{sc} = 1.4$ mA/cm^2. We believe that the smaller projected area corresponding primarily to the i-segment is the best measure of the device performance, because of the short depletion widths and minority carrier diffusion lengths in the heavily doped p- and n-regions.
(18) The ideal diode equation under illumination can be written in logarithmic form as[7] $\ln(I_{sc}) = (q/nkT)V_{oc} + \ln(I_0)$ where n is the diode ideality factor, q is fundamental charge, k is Boltzmann's constant, and I_0 is the saturation current. The slope and intercept of the line are used to determine n and I_0, respectively. I_{sc} is linearly dependent upon the number of photo-generated carriers and therefore the illumination intensity. It follows from the equation that V_{oc} will depend logarithmically on intensity (Figure 3A).
(19) Huynh, W. U.; Dittmer, J. J.; Alivisatos, A. P. *Science* **2002**, *295*, 2425.
(20) Law, M.; Greene, L. E.; Johnson, J. C.; Saykally, R.; Yang, P. *Nat. Mater.* **2005**, *4*, 455.
(21) Green, M. A. *Prog. Photovolt. Res. Appl.* **2003**, *11*, 333.
(22) Wurfel, P. *Physics of Solar Cells, From Principles to New Concepts*; Wiley-VCH: Weinheim, 2005.
(23) Ambrosone, G.; Coscia, U.; Murri, R.; Pinto, N.; Ficcadenti, M.; Morresi, L. *Solar Energy Materials and Solar Cells* **2005**, *87*, 375.

NL8023438